Neuron

Article

Sequential inhibitory plasticities in hippocampal area CA2 and social memory formation

Graphical abstract

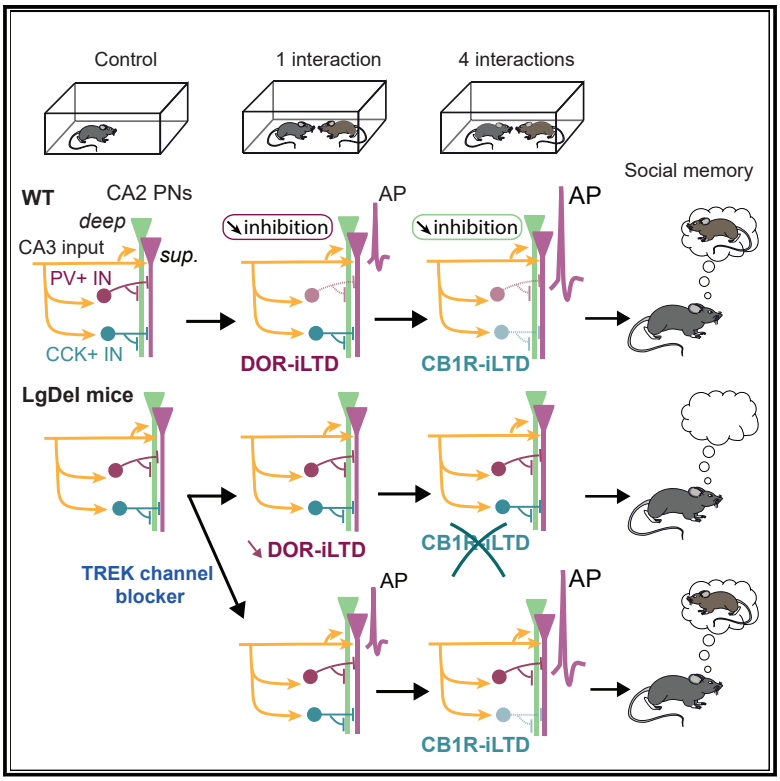

Highlights

- CB1R induces a long-term depression at inhibitory synapses in hippocampal area CA2
- CB1R-LTD induction requires action potential firing in CA2 pyramidal neurons
- CB1R-LTD is induced by social interactions and is required for social memory
- CB1R-LTD is impaired in the 22q11.2 mouse model of schizophrenia

Authors

Maïthé Loisy, Guillaume Bouisset, Sébastien Lopez, ..., Rebecca Ann Piskorowski, Laure Verret, Vivien Chevaleyre

Correspondence

vivien.chevaleyre@u-paris.fr

In brief

Social recognition is important for gregarious animals. In this issue of *Neuron*, Loisy et al. describe a plasticity induced by CB1R that contributes to social memory formation. This plasticity is impaired in a mouse model of schizophrenia but is rescued by manipulation that rescues social memory in these mice.

Loisy et al., 2022, Neuron *110*, 2854–2866
September 7, 2022
https://doi.org/10.1016/j.neuron.2022.06.013

CellPress

CellPress

Neuron

Article

Sequential inhibitory plasticities in hippocampal area CA2 and social memory formation

Maïthé Loisy,[1] Guillaume Bouisset,[3] Sébastien Lopez,[3] Maud Muller,[1] Alena Spitsyn,[1] Jeanne Duval,[1] Rebecca Ann Piskorowski,[1,2] Laure Verret,[3] and Vivien Chevaleyre[1,2,4,*]

[1]Université Paris Cité, INSERM U1266, Institute of Psychiatry and Neuroscience of Paris, 75014 Paris, France
[2]GHU Paris Psychiatrie et Neurosciences, France
[3]Research Center on Animal Cognition, Center for Integrative Biology, Toulouse University, CNRS, UPS, 31062 Toulouse, France
[4]Lead contact
*Correspondence: vivien.chevaleyre@u-paris.fr
https://doi.org/10.1016/j.neuron.2022.06.013

SUMMARY

Area CA2 is a critical region for diverse hippocampal functions including social recognition memory. This region has unique properties and connectivity. Notably, intra-hippocampal excitatory inputs to CA2 lack canonical long-term plasticity, but inhibitory transmission expresses a long-term depression mediated by Delta-opioid receptors (DOR-iLTDs). Evidence indicates that DOR-iLTDs are insufficient to underlie social coding. Here, we report a novel inhibitory plasticity mediated by cannabinoid type 1 receptor activation (CB1R-iLTD). Surprisingly, CB1R-iLTD requires previous induction of DOR-iLTDs, indicating a permissive role for DOR plasticity. Blockade of CB1Rs in CA2 completely prevents social memory formation. Furthermore, the sequentiality of DOR- and CB1R-mediated plasticity occurs *in vivo* during successive social interactions. Finally, CB1R-iLTD is altered in a mouse model of schizophrenia with impaired social cognition but is rescued by a manipulation that also rescues social memory. Altogether, our data reveal a unique interplay between two inhibitory plasticities and a novel mechanism for social memory formation.

INTRODUCTION

The hippocampus is a critical structure for episodic memory formation, and much is known about many of the cellular properties underlying spatial encoding (Mehta, 2015). Lesioning studies have shown that area CA2 is a critical region for social memory formation (Stevenson and Caldwell, 2014; Hitti and Siegelbaum, 2014). Furthermore, increasing vasopressin release in area CA2 during social interaction strongly enhanced the duration of social memory (Smith et al., 2016). Because intra-hippocampal excitatory inputs between CA3 and CA2 do not express long-term plasticity under basal conditions (Chevaleyre and Siegelbaum, 2010; Zhao et al., 2007), it was proposed that plasticity of inhibitory transmission could contribute to memory formation. Indeed, inhibitory transmission from parvalbumin-expressing interneurons (PV+ INs) in area CA2 expresses a unique long-term depression (iLTD) mediated by Delta-opioid receptor (DOR) activation (Piskorowski and Chevaleyre, 2013a). This plasticity emerges during adolescence parallel with the emergence of social memory (Domínguez et al., 2019). Furthermore, pharmacological blockade of DORs (Leroy et al., 2017) or down-regulation of DOR expression (Domínguez et al., 2019) reduces social memory.

Area CA2 is particularly vulnerable in the context of psychiatric disease. Human postmortem studies of schizophrenic and bipolar patients have reported a decrease in PV+ INs specifically in hippocampal area CA2 (Benes et al., 1998; Knable et al., 2004). There is also a decrease in PV+ IN density specifically in area CA2 in a mouse model of 22q11.2 deletion syndrome (DS) (Piskorowski et al., 2016), one of the highest genetic factors for developing schizophrenia (Karayiorgou et al., 2010). Social memory formation and DOR plasticity were strongly impaired in these mice (Piskorowski et al., 2016), suggesting that impairment in DOR plasticity might underlie deficits in social memory in psychiatric disorders. In this study, we provide evidence that DOR plasticity is permissive for the induction of another inhibitory plasticity mediated by cannabinoid type 1 receptors (CB1Rs). We further explore how this CB1R-mediated plasticity participates in social memory formation.

RESULTS

DOR-iLTD is permissive for CB1R-mediated plasticity

We hypothesized that following induction of DOR-iLTD in area CA2, the depression of the PV-CA2 PN (pyramidal neuron) synapses may allow the expression of a secondary synaptic

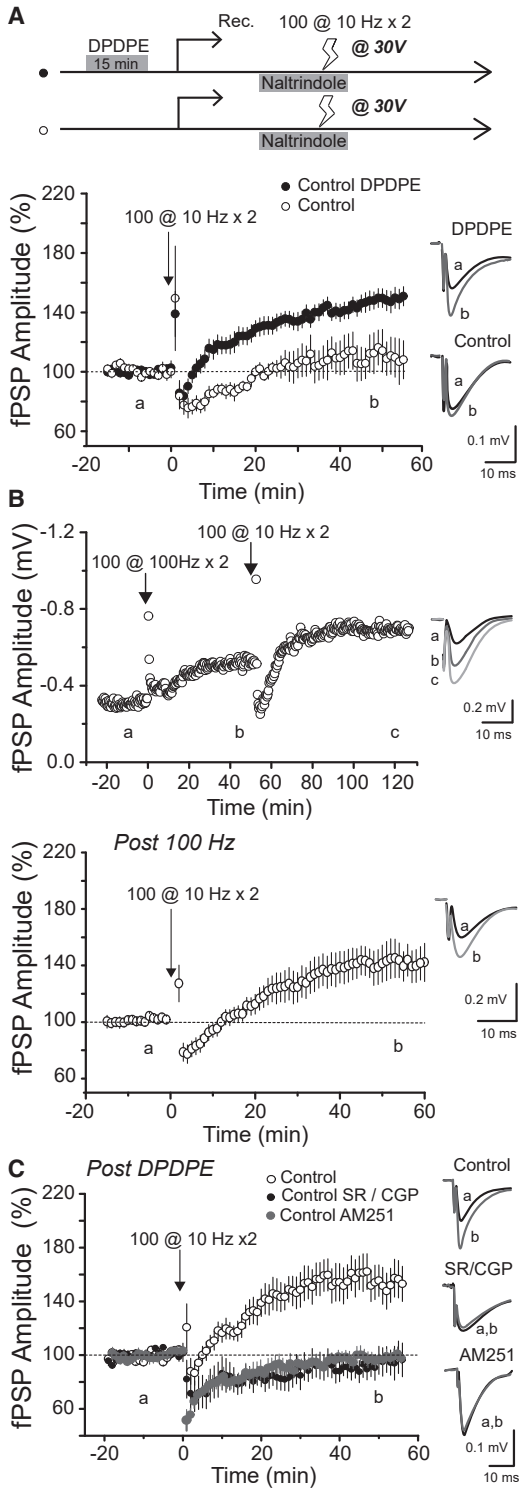

Figure 1. DOR-mediated plasticity is permissive for CB1R-mediated plasticity

(A) Top: diagram illustrating the experimental protocol. Before undergoing the recording protocol, slices were incubated in artificial cerebral spinal fluid (ACSF) with or without the delta opioid receptor (DOR) agonist DPDPE (0.5 μM) for 20 min. A 10 Hz stimulation (100 pulses at 10 Hz repeated twice) was applied to induce plasticity in the presence of the DOR antagonist Naltrindole (0.1 μM). The stimulus intensity was increased to 30V only during the 10 Hz stimulation. Bottom: time course of normalized fPSP amplitude with prior DPDPE incubation (filled circles, n = 18, p = 8.2 10^{-7}) or in control (open circles, n = 7, p = 0.348). Right: averaged sample fPSP traces corresponding to the time points before (a) and after (b) 10 Hz stimulation.

(B) Top: representative experiment of CA3-CA2 fPSP amplitude in which DOR-mediated plasticity was induced with a high frequency stimulation (HFS; 100 pulses at 100 Hz repeated twice) and then a 10 Hz stimulation protocol was provided (at 30V). Bottom: summary graph showing the effect of the 10 Hz stimulation provided 50–60 min after the 100 Hz stimulation (n = 11, p = 6.7 10^{-4}). Right: averaged fPSP traces.

(C) Summary graph of normalized CA3-CA2 fPSP recorded before and after a 10 Hz stimulation at 30V. The increase in fPSP in control (open circles, n = 13, p = 2.4 10^{-4}) was blocked by $GABA_{A/B}$ receptor blockers SR95531 (1 μM)/CGP55845 (2 μM; black-filled circles, n = 5, p = 0.64) and by the CB1R inverse agonist AM251 (4 μM; gray-filled circles, n = 5, p = 0.75). Right: averaged fPSP traces. Error bars denote SEM See also Figure S1.

plasticity. We found that following a 20-min incubation of hippocampal slices in the DOR agonist DPDPE, delivery of an electrical stimulation of CA3 inputs (2 trains of 100 pulses at 10 Hz at 20V–30V stimulus intensity) evoked a lasting increase in the field post synaptic potential (fPSP) amplitude in CA2 (Figure 1A; 147.0% ± 6.0%, n = 18, p = 8.2 10^{-7}). When slices were not incubated in DPDPE, no significant increase in fPSP was observed following a 10 Hz stimulation (Figure 1A; 109.8% ± 9.6%, n = 7, p = 0.348). The 10 Hz stimulation was performed in the presence of the DOR antagonist Naltrindole, indicating that the lasting increase is not due to further DOR activation. Accordingly, a 10 Hz stimulation provided after DPDPE incubation had an identical effect whether it was provided with or without Naltrindole (Figure S1). This result suggests that DOR-iLTD is permissive for another plasticity.

Next, we predicted that this plasticity will be present following a 100 Hz electrical stimulation, a protocol that is also effective to evoke DOR-iLTD (Piskorowski and Chevaleyre, 2013a). In basal conditions, CA3 excitatory inputs do not express long term potentiation (LTP) in area CA2, and the increase in fEPSP amplitude induced by DOR activation is entirely dependent on DOR-iLTD (Nasrallah et al., 2015). Induction of DOR-iLTD with a 100 Hz electrical stimulation resulted in a long-term increase in the fPSP amplitude (Figure 1B; 130.3% ± 1.4%, n = 11, p = 6.7 10^{-4}). In the same slices, we observed a further increase in the fPSP amplitude following a 10 Hz stimulation at 30V (Figure 1B; 40.8% ± 10.7%, n = 11, p = 9.77 10^{-4}) that was not different from that induced by a 10 Hz stimulation after incubation in DPDPE (p = 0.62).

We next wondered whether the second increase in fPSP amplitude is due to LTP of excitatory transmission or is caused by further LTD at inhibitory synapses. In the presence of $GABA_{A/B}$ receptor (GABAR) blockers (SR95531/CGP55845) the 10 Hz protocol did not result in any lasting increase in the fPSP amplitude (Figure 1C; 96.3% ± 11.1%, n = 5, p = 0.64), in contrast to interleaved control experiments (Figure 1C; 159.3% ± 12.7%, n = 13, p = 2.4 10^{-4}). We thus conclude that the increase in fPSP amplitude following a 10 Hz stimulation is entirely dependent on a change in inhibitory transmission.

In area CA1, inhibitory transmission undergoes an iLTD that depends on cannabinoid type 1 receptor (CB1R) activation (Chevaleyre and Castillo, 2003). We found that in the presence of the

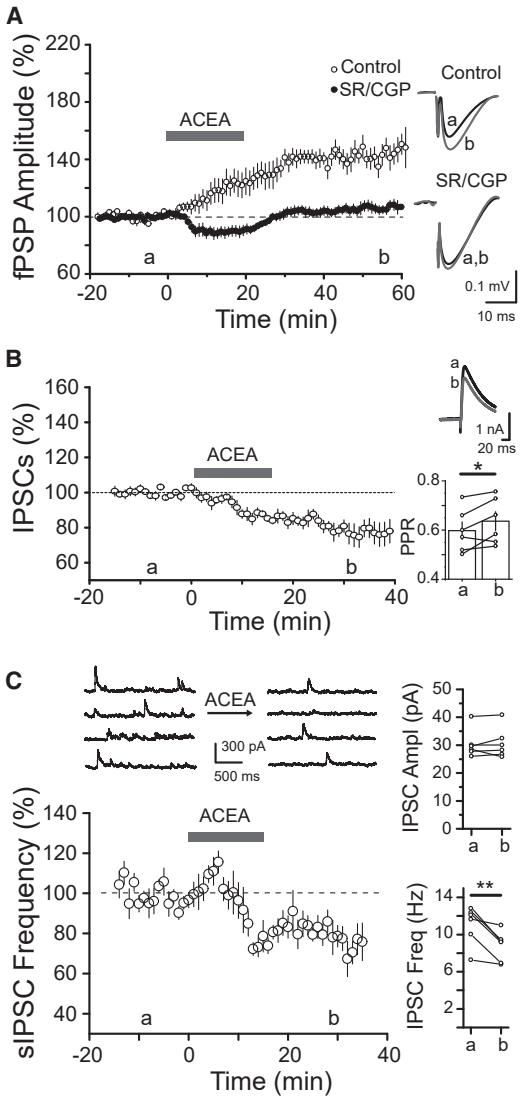

Figure 2. Activation of CB1Rs decreases GABA release and disinhibits CA3-CA2 excitatory transmission

(A) Summary graph of normalized CA3-CA2 fPSP amplitude before and after application of the CB1R agonist ACEA (15 μM) in control (open circles, n = 6, p = 6.8 10^{-4}) and in presence of $GABA_{A/B}$ receptor blockers (SR95531/CGP55845; filled circles, n = 10, p = 0.353). Right: averaged fPSP traces corresponding to the time points before (a) and after (b) ACEA application.

(B) Summary graph showing the effect of ACEA on IPSC amplitude in the presence of AMPA/NMDA receptor blockers (NBQX/AP-V, 10 and 25 μM respectively, n = 6, p = 0.009). Top right: averaged IPSC traces. Bottom right: the paired-pulse ratio (PPR) for individual experiments before (a) and after (b) ACEA application. Cells were held at +10 mV throughout the experiment.

(C) Top: example traces of spontaneous IPSCs (sIPSCs) recorded in a CA2 PN before and after application of ACEA. Bottom: summary graph of sIPSC frequency during application of ACEA. Right: ACEA induced a significant decrease in sIPSC frequency (n = 6, p = 0.031) but did not affect sIPSC amplitude (n = 6, p = 0.92). Error bars denote SEM.

CB1R inverse agonist AM251, the 10 Hz protocol in CA2 did not result in any lasting change in fPSP amplitude (Figure 1C; 98.3% ± 4.0%, n = 5, p = 0.75). Altogether, these data show that DOR-mediated plasticity is permissive for the induction of a secondary inhibitory plasticity that requires CB1R activation.

Activation of CB1R induces an iLTD and a disinhibition of CA3-CA2 excitatory transmission

If CB1R activation modulates inhibitory transmission in area CA2, application of a CB1R agonist should result in an increase in the fPSP amplitude. We found that a transient application of the CB1R agonist ACEA induced a lasting increase in the fPSP amplitude (Figure 2A; 144.5% ± 5.5%, n = 6, p = 6.8 10^{-4}). This increase was entirely mediated through a decrease in inhibitory transmission because it was prevented by GABAR blockers (Figure 2A; 104.6% ± 5.0%, n = 10, p = 0.353).

Next, we performed whole-cell voltage-clamp recording to monitor inhibitory post synaptic potentials (IPSCs) at +10 mV in the presence of AMPA/NMDA receptor blockers (D-AP5 and NBQX). Application of ACEA induced a lasting decrease in IPSC amplitude (Figure 2B; 78.5% ± 5.3%, n = 6, p = 0.009). In the hippocampus, CB1Rs are mostly expressed at GABAergic terminals where they act to decrease neurotransmitter release (Chevaleyre et al., 2006). Accordingly, ACEA application resulted in a significant increase in the paired-pulse ratio (PPR) of two successive IPSCs, a measure inversely correlated with release probability (Figure 2B; from 0.60 ± 0.04 to 0.64 ± 0.04, n = 6, p = 0.043). In addition, ACEA application also induced a decrease in spontaneous IPSC frequency (Figure 2C; 80.7% ± 4.4%; from 10.98 ± 0.83 to 8.78 ± 0.66 Hz, n = 6, p = 0.031) but did not change their amplitude (from 30.4 ± 2.1 to 30.7 ± 2.3 pA, n = 6, p = 0.92). These data are consistent with the presynaptic location of CB1Rs and indicate that CB1R activation induces a decrease in GABA release probability.

CA2 PN action potential firing is necessary and sufficient to induce CB1R plasticity

Next, we investigated potential cellular mechanisms involved in the induction of CB1R-mediated plasticity in area CA2. We found that while the 10 Hz stimulation protocol at 30V was efficient to trigger a lasting increase in fPSP amplitude (Figure 3A; 136.8% ± 2.8%, n = 8, p = 7.96 10^{-6}), the same stimulation at 10V had little effect (Figure 3A; 109.5% ± 3.6% of baseline, n = 7, p = 0.032). Furthermore, in contrast to DOR-iLTD that can be induced with a 100 Hz stimulus, a 100 Hz stimulation failed to induce any significant increase in fPSP amplitude following DPDPE incubation (Figures S2A and S2B; 106.8% ± 5.4%, n = 5, p = 0.28). Likewise, a 1 Hz stimulation protocol did not trigger any significant increase in fPSP amplitude (Figures S2A and S2B; 104.5% ± 3.3%, n = 5, p = 0.18). One possible explanation for these findings is that CB1R plasticity may require CA2 PNs to fire action potentials (APs) for induction. Indeed, CA3 inputs do not evoke APs in CA2 PNs in basal conditions (Piskorowski and Chevaleyre, 2013b), but they do following DOR-iLTD (Nasrallah et al., 2015).

Thus, we tested whether AP firing by CA2 PNs was sufficient to evoke this plasticity using whole-cell recording of PNs. We monitored the depolarizing component of the CA3-CA2 PSPs at −70 mV and then evoked APs directly in the recorded cell with injected current steps at 10 Hz. This protocol evoked a large and lasting increase in the depolarizing component of the

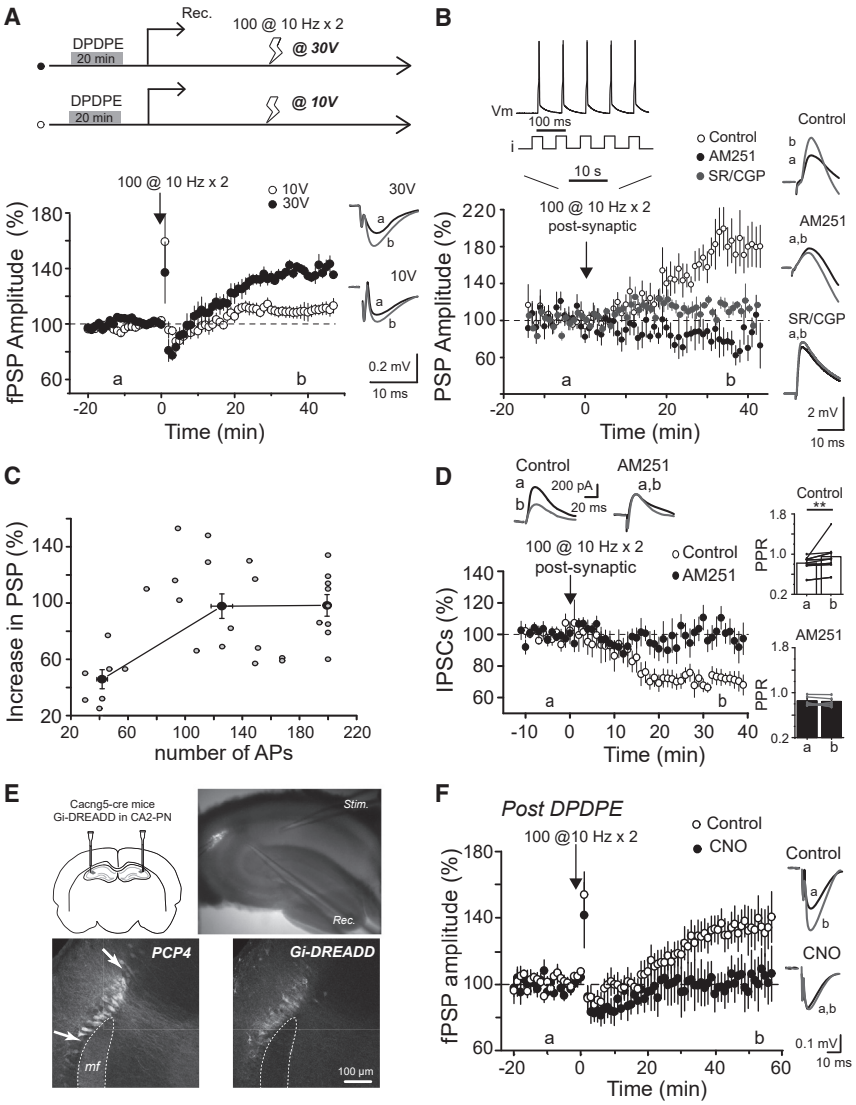

Figure 3. CA2 PN AP firing is sufficient to induce CB1R-mediated plasticity

(A) Top: diagram illustrating the experimental protocol. Bottom: summary graph of normalized CA3-CA2 fPSP before and after 10 Hz stimulation at 30V (filled circles, n = 8, p = 7.96 10^{-6}) and at 10V (open circles, n = 7, p = 0.032). Right: averaged fPSP example traces corresponding to the time points before (a) and after (b) 10 Hz stimulation.

(B) Summary graph of normalized CA3-CA2 PSP amplitude recorded in whole-cell current-clamp configuration before and after a post-synaptic 10 Hz stimulation (100 depolarizing steps of 7 ms provided at 10 Hz, repeated twice). APs induced by the 10 Hz stimulation provide a lasting increase in PSP (open circles, n = 18, 0.013) that was blocked by AM251 (filled circles, n = 10, p = 0.346) and by GABAA/B receptor blockers (SR95531/CGP55845; gray-filled circles, n = 6, p = 0.09). Right: averaged PSP traces. Cells were held at −70 mV throughout the experiment.

(C) Graph showing the magnitude of increase in the PSP amplitude (percentage of increase from baseline) plotted as a function of AP number induced by post-synaptic 10 Hz stimulation (n = 7, p = 5.1 10^{-4}).

(D) Top: averaged IPSC traces. Bottom: summary graph showing the effect of post-synaptic 10 Hz stimulation on IPSC amplitude in control (open circles, n = 8, p = 3.16 10^{-4}) and in presence of AM251 (filled circles, n = 5, p = 0.968). Right: PPR for individual experiments before (a) and after (b) 10 Hz stimulation. Cells were held at −70 mV throughout the experiment.

(E) Cacng5-cre mice were injected in CA2 with AAV allowing cre-dependent expression of Gi-DREADD-mCherry. The recorded hippocampal slice shows fluorescence in area CA2. This panel also shows confocal image of the same slice after staining for PCP4 and mCherry. Scale bar is 100 µm.

(F) Summary graph of normalized CA3-CA2 fPSP amplitude before and after 10 Hz stimulation provided in absence of CNO (open circles, n = 8, p = 0.0078) or in presence of CNO (10 µM; filled circles, n = 7, p = 0.86). Right: averaged fPSP example traces. Error bars denote SEM in all panels. See also Figure S2.

EPSP-IPSP sequence (Figure 3B; 176.2% ± 17.1%, n = 18, p = 0.0013). This increase was dependent on inhibitory transmission because it was blocked by GABAR blockers (Figure 3B; 115.0% ± 7.35%, n = 6, p = 0.09). It was also dependent on CB1R activation because it was prevented by AM251 (Figure 3B; 90.8% ± 12.4%, n = 10, p = 0.346). These experiments were performed without prior DOR-iLTD induction, demonstrating that AP firing alone is sufficient to induce CB1R plasticity. Then, we plotted the number of APs that were evoked during the induction protocol versus the percentage of plasticity. We found that a significant increase of PSP amplitude was induced with 30–60 APs (Figure 3C; 45.8% ± 6.8%, n = 7, p = 5.1 10^{-4}). Increasing the number of APs increased the magnitude of the plasticity with an apparent plateau at ~100 APs (97.8% ± 8.7%), resulting in an increase in PSP amplitude similar to that evoked with 200 APs (98.3% ± 7.7%).

To directly measure changes in inhibitory transmission, we recorded IPSC amplitude at −70 mV. In order to induce CB1R-iLTD, we transiently switched to current clamp during the induction protocol to evoke APs. We found that 10 Hz AP firing in the PN induced an LTD of IPSC amplitude (Figure 3D; 70.9% ± 4.2%, n = 8, p = 3.16 10^{-4}) that was prevented by AM251 (99.8% ± 7.7%, n = 5, p = 0.968). Furthermore, iLTD induction resulted in a significant increase in the PPR of two successive IPSCs (Figure 3D; from 0.82 ± 0.05 to 0.95 ± 0.11, n = 8, p = 0.0078) that was prevented by AM251 (Figure 3C; from 0.85 ± 0.04 to 0.84 ± 0.04, n = 5, p = 0.84).

These experiments show that AP firing in CA2 PNs is sufficient to induce CB1R-iLTD. The CB1R plasticity likely relies on the ability of DOR-iLTD to reveal AP firing in PNs upon CA3 input stimulation. To directly address this, we performed two experiments. First, we performed whole-cell recording and prevented

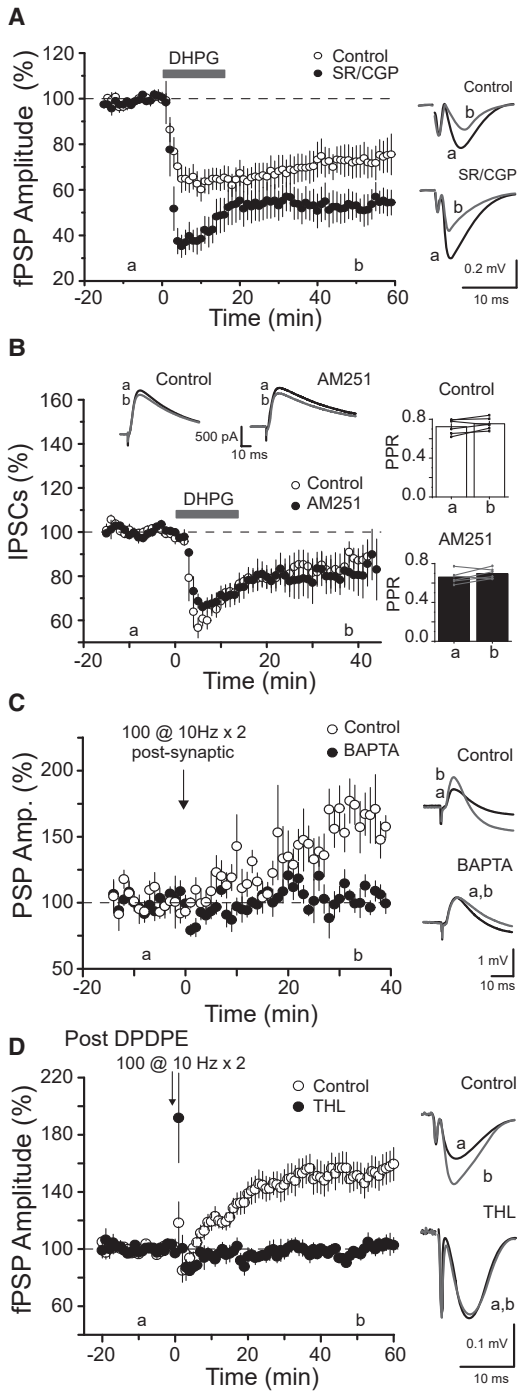

Figure 4. eCB release in area CA2 depends on Ca^{2+} increase and DAG-L but not on mGluR-I activation

(A) Summary graph of normalized CA3-CA2 fPSP amplitude showing the effect of a 10 min application of mGluR-1 receptor agonist DHPG (50 μM) in the presence of GABAR blockers (SR95531/CGP55845; filled circles, n = 6, n = 3.98 10^{-4}) or in control condition (open circles, n = 9, p = 0.0046). Right: averaged sample fPSP traces corresponding to the time points before (a) and after (b) DHPG application.

(B) Summary graph of IPSCs recorded in the presence of AMPA and NMDA receptor blockers showing the effect of DHPG application in control conditions (open circles, n = 6, p = 0.058) or in presence of AM251 (filled circles, n = 6, p = 0.05). Top: averaged IPSC traces. Right: PPR for individual experiments before (a) and after (b) DHPG application. Cells were held at +10 mV throughout the experiment.

(C) Summary graph of normalized CA3-CA2 PSP recorded in whole-cell before and after a post-synaptic stimulation. APs induced by the 10 Hz stimulation led to a lasting increase in PSP amplitude (open circles, n = 11, p = 2.8 10^{-4}) in control but not with intracellular BAPTA (20 mM) (filled circles, n = 7, p = 0.146). Right: averaged PSP traces. Cells were held at −70 mV throughout the experiment.

(D) Summary graph of normalized CA3-CA2 fPSP before and after a 10 Hz electrical stimulation. Stimulation induced a lasting increase in fPSP in control conditions (open circles, n = 16, p = 3.05 10^{-5}) but not in the presence of the DAG-L inhibitor THL (10 μM; filled circles, n = 7, p = 0.939). Right: averaged fPSP traces. Error bars indicate the SEM in all panels. See also Figure S3.

AP firing by injecting hyperpolarizing current during the 10 Hz stimulation of CA3 inputs. We simultaneously recorded the fPSP to ensure that the disinhibitory plasticity was induced. We observed no plasticity in the absence of AP firing (Figures S2C and S2D, 104% ± 16.6%, n = 10, p = 0.74) even with plasticity present in the same slice (Figure S2D, 137.1% ± 8.8%, n = 10, p = 0.002). Next, we expressed inhibitory DREADDs in CA2 PNs using the CACNG5-cre mouse line (Boehringer et al., 2017). In slices incubated in DPDPE, a 10 Hz stimulation of CA3 inputs after application of clozapine N-oxide (CNO) did not induce any plasticity (Figures 3E and 3F; 102.2% ± 13.4%, n = 7, p = 0.86), in contrast to 10 Hz stimulation in slices expressing DREADDs but without CNO application (133.9% ± 10.9%, n = 8, p = 0.0078). Altogether, these results show that AP firing in CA2 PNs is necessary and sufficient to evoke CB1R-iLTD.

CB1R-mediated plasticity depends on calcium increase in PNs and diacylglycerol lipase activation but not on mGluR-I activation

In area CA1, CB1R-iLTD is induced after SC stimulation by activation of group I metabotropic glutamate receptors (mGluR-Is) that trigger the release of the endocannabinoid (eCB) 2-arachidonoylglycerol (2-AG) independently of intracellular [Ca^{2+}] (Chevaleyre and Castillo, 2003). To determine if a similar mechanism is present in CA2 PNs, we looked at the effect of the mGluR-I agonist DHPG on fPSPs. When GABARs were blocked, DHPG induced a large and long-lasting depression of the fEPSP (Figure 4A; 53.7% ± 5.6%, n = 6, p = 3.98 10^{-4}). When DHPG was applied in slices with intact inhibitory transmission, the depression of the fPSP was smaller (Figure 4A; 75.6% ± 6.3%, n = 9, p = 0.0046), suggesting that inhibitory transmission might also be decreased by DHPG. Therefore, we directly monitored IPSCs at +10 mV and tested the effect of DHPG. DHPG application induced a transient decrease of the IPSC amplitude followed by a smaller but lasting depression (Figure 4B; 83.3% ± 6.72%, n = 6, p = 0.058). In the presence of AM251, DHPG application induced a similar depression of the IPSCs (Figure 4B; 81.3% ± 7.3%, n = 6, p = 0.050). In both conditions, DHPG induced a non-significant increase in the PPR (control: from 0.72 ± 0.03 to 0.75 ± 0.02, n = 6, p = 0.138; in AM251: from 0.66 ± 0.03 to 0.70 ± 0.02, n = 6, p = 0.169). These data show that mGluR-I activation decreases inhibitory transmission in

area CA2 but in a CB1R-independent manner. We also tested whether 10 Hz-induced CB1R plasticity is altered after blocking all mGluRs. We found that in the presence of CPPG and MCPG, the magnitude of the plasticity was identical to that observed in control experiments (Figure S3A, 158.9% ± 6.7%, n = 5, p = 0.001). Therefore, in area CA2, mGluRs are likely not required for CB1R-mediated plasticity.

Next, we tested whether CB1-plasticity is altered after chelating Ca^{2+} in CA2 PNs. With BAPTA in the recording pipette, the induction of the disinhibitory increase in PSP amplitude by post-synaptic 10 Hz stimulation was completely abolished (Figure 4C; 107.1% ± 4.5%, n = 7, p = 0.146), while an increase in PSP was observed in interleaved recordings without BAPTA (Figure 4C; 165.7% ± 10.8%, n = 11, p = 2.8 10^{-4}). Altogether, these results support the conclusion that an increase in intracellular [Ca^{2+}] during AP firing is a requirement for CB1R-iLTD induction, likely leading to eCB release.

In area CA1, eCB release after CA3 input stimulation is extremely localized, giving this plasticity an input specificity. Because eCB release in area CA2 requires AP-induced increase in intracellular [Ca^{2+}], it is possible that in CA2, CB1R-iLTD will not be input specific. To test this, we placed two stimulation pipettes in stratum radiatum (SR) ~200 μm apart from each other (Figure S3B) and verified that the two stimulated pathways were independent. We evoked PSPs from both inputs before and after delivering a 10 Hz stimulation to only one pathway. The 10 Hz stimulation protocol resulted in a large increase in fPSP amplitude in the pathway where it was delivered (Figures S3B and S3C; 139.5% ± 5.2%, n = 7, p = 3.1 10^{-4}), as well as in the other pathway that did not undergo the induction protocol (Figures S3B and S3C; 142.0% ± 9.4%, n = 7, p = 0.0028). This result shows that in contrast to CA1 PNs, expression of CB1R-iLTD in CA2 PNs is not input specific.

We then wanted to determine which eCB is involved in CB1R plasticity in area CA2. In area CA1, both iLTD and the short-term decrease in inhibitory transmission have been ascribed to the release of 2-AG. We found that when the diacylglycerol lipase (DAG-L) inhibitor tetrahydrolipstatin (THL) was applied to slices, a 10 Hz stimulation did not induce any lasting increase in fPSP amplitude (Figure 4D; 100.4% ± 3.3%, n = 7, p = 0.939), in contrast to interleaved controls (157.2% ± 10.6%, n = 16, p = 3.05 10^{-5}). Therefore, we conclude that 2-AG is likely the eCB released during the plasticity in area CA2.

CB1R-iLTD targets CCK+ interneurons and increases AP firing in deep CA2 PNs

In order to examine how AP firing is altered in area CA2 following CB1R-iLTD, we performed extracellular recordings to monitor population spikes (PSs) in the pyramidal layer of CA2. We observed a PS after CA2 slices were incubated in DPDPE. The PS amplitude was increased further following a subsequent 10 Hz electrical stimulation (Figure 5A; at 30V: Stim 1: from 102.2 ± 16.4 to 226.1 ± 37.4 μV, n = 8, p = 0.009). Therefore, we conclude that the emergence of AP firing induced by DOR-iLTD at PV + INs can be further increased by induction of CB1R-iLTD.

Although DOR-iLTD is observed by whole-cell recording on all CA2 PNs, not all CA2 PNs are able to fire APs following DOR plasticity (Nasrallah et al., 2019). Therefore, we postulated that only cells that fire APs after DOR plasticity would express CB1R plasticity. To address this in a minimally invasive way, we performed cell-attached recordings to detect AP firing in response to CA3 input stimulation. We first induced DOR plasticity by applying DPDPE and measured AP firing probability. As expected, only a fraction of cells fired APs following DPDPE application (8 out of 15; Figure 5B). Then we applied a 10 Hz stimulation of CA3 inputs and again measured the AP firing probability. Consistent with our prediction, the cells that did not fire APs following DPDPE were unlikely to fire APs following the 10 Hz stimulation (Figure 5B; at 30V: Stim 1: from 0.021 ± 0.021 to 0.068 ± 0.046, n = 7, p = 0.5). However, the cells that fired APs after DOR activation showed a significant increase in AP firing probability following the 10 Hz stimulation (Figure 5B; at 30V: Stim 1: from 0.406 ± 0.084 to 0.716 ± 0.085, n = 8, p = 0.039).

Because we observed a fraction of CA2 PNs that fired APs following DPDPE application, we asked if these cells might have a preferential location. To answer this, we evoked DOR plasticity with DPDPE and then performed cell-attached recordings. Following the recording, we filled the cells with Alexa Fluor 594 Cadaverine and performed post hoc analysis of the somatic location with confocal imaging. Interestingly, the vast majority of PNs that fired APs after DOR plasticity were located in the superficial layer, closer to SR (13 out of 25), while only 1 out of 28 PNs in the deep layer (closer to SO) was firing APs (Figures 5C and 5D).

While deep PNs do not fire APs after DPDPE in response to two stimulations of CA3 input, it is still possible that they fire enough APs during the 10 Hz stimulation to express CB1R plasticity. With cell-attached recordings, we quantified the number of APs evoked during the 10 Hz stimulation. This stimulation evoked 162.9 ± 14.3 APs in superficial cells (Figure 5E; n = 14), but only 38.3 ± 18.6 APs in deep cells (n = 12). Therefore, it is likely that deep PNs express little or no CB1R plasticity after the 10 Hz protocol. We also quantified AP firing with the 100 Hz stimulation and found that both superficial and deep cells fired very few APs (respectively 15.2 ± 4.2, n = 25 and 4.1 ± 1.6 APs, n = 34), thus explaining why 100 Hz stimulation is not efficient to induce CB1R-mediated plasticity.

In the hippocampus, CB1Rs are expressed by cholecystokinin-expressing interneurons (CCK+ INs; Katona et al., 1999). To confirm that CCK+ INs are indeed targeted by CB1R plasticity, we made use of the fact that GABA release from PV+ and CCK+ INs is mediated by different voltage-activated calcium channels (Ca_V) (respectively P/Q and N-type) (Hefft and Jonas, 2005). We blocked N-type Ca_V channels with ω-Conotoxin GVIA and then evoked CB1R plasticity with direct AP firing at 10 Hz to prevent plasticity induction failure due to a potential decrease in CA3 transmission. After blocking N-type channels, the 10 Hz protocol did not induce the CB1R plasticity (Figures S4A and S4C: 90.0% ± 11.5%, n = 6, p = 0.56), showing that CCK+ INs are likely the target of CB1R plasticity. Because PV+ and CCK+ INs can interact in CA1 (Dudok et al., 2021), we also wondered whether PV+ INs play a role in this plasticity. We used viral injection to express inhibitory DREADDs in a PV-cre mouse line. We found that silencing PV+ transmission with CNO did not affect the disinhibitory

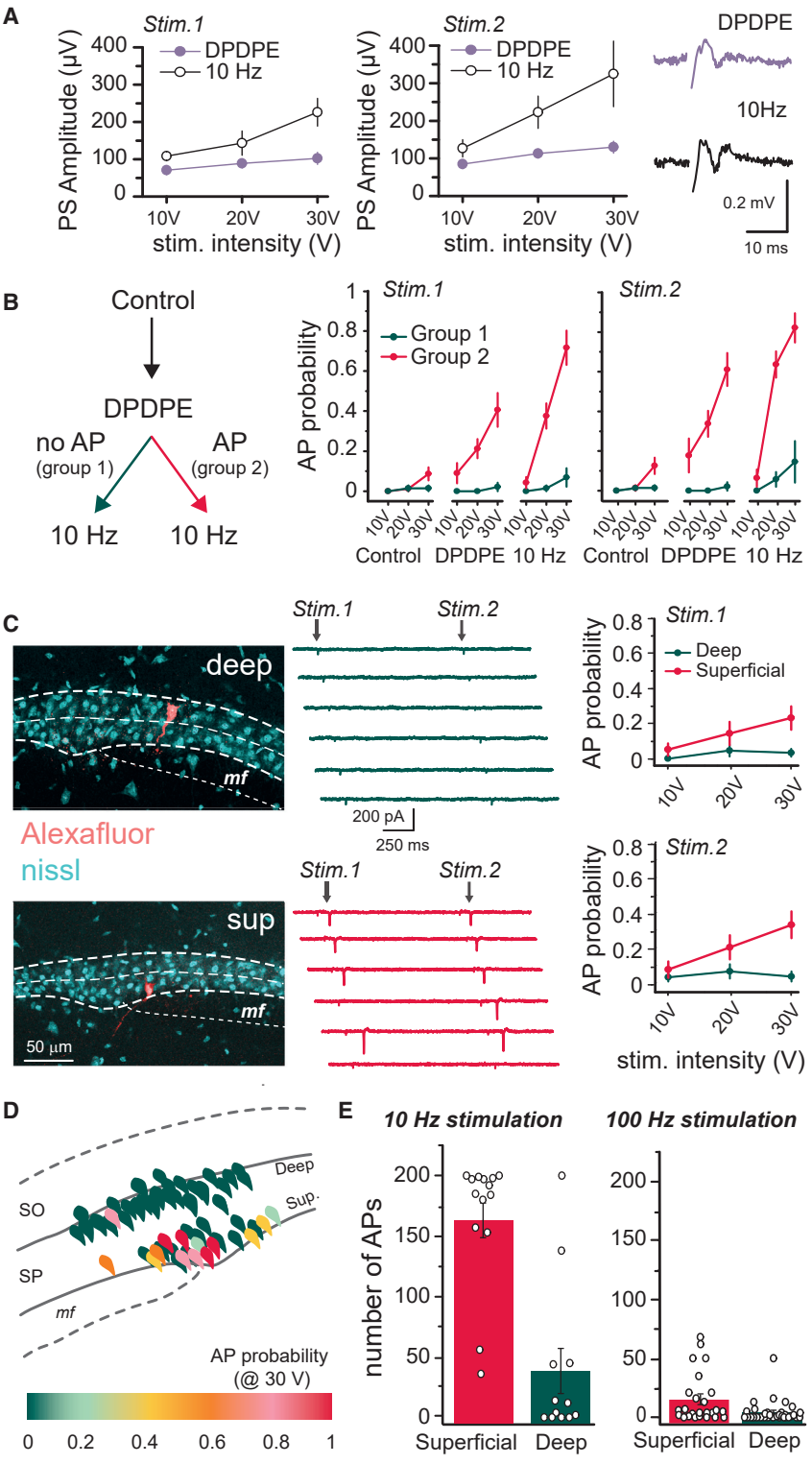

Figure 5. CB1R-iLTD increases AP firing specifically in CA2 PNs that are firing APs after DOR-iLTD

(A) Summary graphs of the population spike amplitude monitored in the somatic layer of area CA2 in response to a paired SC input stimulation after DPDPE application (0.5 μM; purple-filled circles, n = 8) and after 10 Hz stimulation (open circles, n = 8). Right: averaged PSP traces corresponding to the time points after DPDPE or 10 Hz stimulation.

(B) Left: diagram illustrating the experimental protocol. AP firing probability was quantified using cell-attached recordings of PNs in control condition, 20 min after DPDPE application, and 20 min after a 10 Hz stimulation of CA3 inputs. Right: summary graphs of AP firing probability in control, after DPDPE, and after 10 Hz stimulation.

(C) Left: sample image of Alexa Fluor-filled PNs located in the deep (top) and superficial (bottom) pyramidal layer. Middle: sample traces of cell-attached recordings following 2 stimulations of CA3 inputs after incubation in DPDPE for the cells shown on the left. Right: summary graph of the AP firing probability for deep PNs (green circles, n = 28) and superficial PNs (red circles, n = 25).

(D) Diagram showing the AP firing probability and location of PN soma.

(E) Summary graph of the number of APs induced by the 10 Hz stimulation in deep (n = 12) and superficial (n = 12) PNs, and number of APs induced by the 100 Hz stimulation in superficial (n = 24) and deep (n = 34) PNs. Error bars denote SEM. See also Figure S4.

CB1-plasticity is involved in social memory formation

Previous studies have suggested that DOR plasticity could be involved in social memory formation, a process dependent on area CA2 (Domínguez et al., 2019; Leroy et al., 2017). To determine if CB1R-iLTD may also play a role in social memory formation, we used several strategies. First, we bilaterally implanted cannulas in dorsal area CA2 (Figure 6A) and delivered either AM251 or vehicle just before the five-trial social memory test (Figure 6B). In mice injected with vehicle, a significant decrease in interaction time with the familiar mouse was observed during trials 2–4 (Figures 6C and 6D: n = 14, p = 0.0025 for trial 4). In contrast, mice injected with AM251 showed no decrease in interaction time on trials 2–4 as compared to trial 1 (Figures 6C and 6D; n = 14, p = 0.986 for trial 4). In both AM251 and vehicle-injected mice, exposure to a novel mouse during the 5th trial led to a level of interaction similar to that which occurred after the first exposure to a new mouse. On the next day, control mice displayed a reduced interaction time with the now-familiar mouse, indicating that social memory was lasting

plasticity induced by AP firing at 10 Hz (Figures S4B and S4C: 199.2% ± 13.7%, n = 5, p = 0.0019). Together, these experiments confirm that CCK+, but not PV+ INs, are the target of CB1R-mediated plasticity.

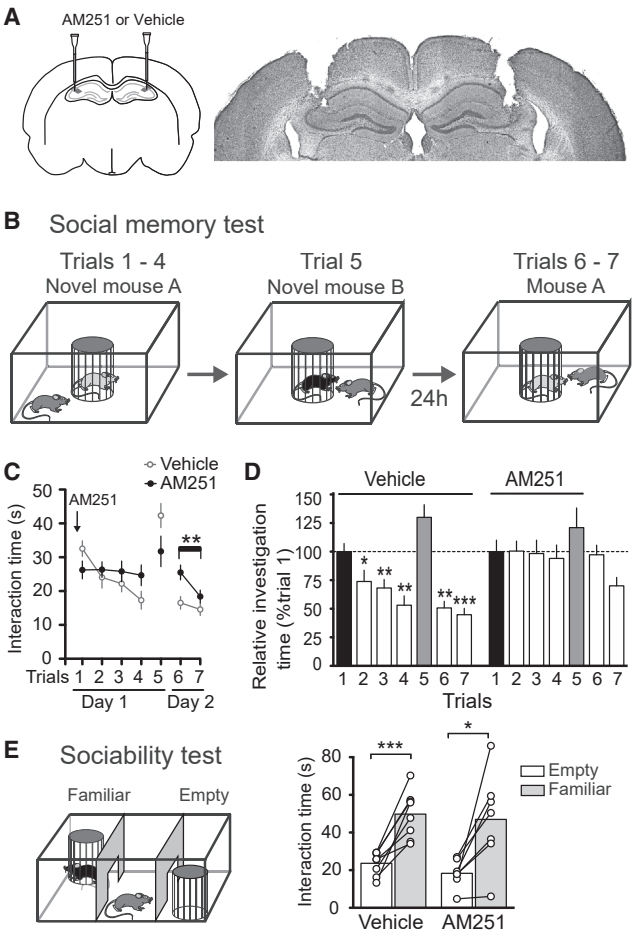

Figure 6. CB1R blockade in area CA2 prevents social memory formation without altering sociability

(A) Diagram illustrating the location of the canulae implantation and micrograph of a brain section confirming proper canulae placement.

(B) Social memory was assessed with the 5-trial test followed the next day by two exposures to the first mouse.

(C and D) Investigation times in mice infused with vehicle decreased significantly from trial 2 to 4 (n = 14, p = 0.0025) and remained decreased on the next day (trials 6–7). In contrast, no significant change in investigation time is observed across trials following AM251 infusion (n = 14, p = 0.968 at trial 4).

(E) Left: diagram of sociability test. Right: plot of interaction times for vehicle-infused control (n = 14, n = 0.0004) and animals infused with AM251 (n = 14, p = 0.0133). Error bars denote SEM See also Figure S5.

at least 24 h. Interestingly, the mice that had been perfused with AM251 the day before showed an interaction time during trial 6 similar to that of trial 1. However, a significant decrease in interaction was observed between trial 6 and 7 (p = 0.0013), suggesting that these mice, now devoid of CB1R blockade in area CA2, were able to form a social memory.

Next, we asked whether the deficit in social memory following AM251 injection could be due to compromised sociability. We found that both vehicle- and AM251-injected mice show a strong preference for a mouse versus an empty chamber (Figure 6E; p = 0.0004 for vehicle and p = 0.0133 for AM251). These data indicate that activation of CB1Rs plays a role in social memory formation, but not in sociability. It has been shown that ventral, but not dorsal, CA3 (Chiang et al., 2018) and CA1 (Meira et al., 2018) are involved in social memory formation. Therefore, it is unlikely that diffusion of AM251 in other dorsal hippocampal areas could explain the deficit in social memory. Accordingly, mice injected with AM251 in dorsal CA1 display a decrease in interaction time that is similar to that of vehicle-injected mice (Figure S5A: n = 7 for both groups, p = 0.06). Furthermore, the locomotion in either CA1 or CA2 AM251-injected mice was not altered compared to that of vehicle-injected mice (Figures S5B and S5C), indicating that lower exploratory activity could not explain the deficit in social memory. Altogether, these results indicate that activation of CB1Rs in area CA2 is required for social memory formation.

If CB1R-iLTD is required for social memory formation, this plasticity might be induced during social interaction. We performed the social memory protocol as before (trials 1–4), then sacrificed the mice 5 min after and studied inhibitory plasticity following social interaction (S.I.). Control mice underwent 4 exposures to the identical environment with no social interaction (Figure 7A). First, we found that the DOR-dependent increase in fPSP amplitude induced by a 100 Hz stimulation was reduced in S.I. mice (Figure 7B; 112.4% ± 5.6%, n = 8, p = 6.66 10^{-4} with control mice) and normal in control mice (147.4% ± 5.9%, n = 9), indicating that DOR plasticity was partially occluded following S.I. Then, we examined if CB1R-mediated plasticity was also altered by S.I. We found that the plasticity induced by a 10 Hz stimulation was significantly smaller in S.I. mice (Figure 7C; 109.2% ± 6.1%, n = 11, p = 5.8 10^{-4} with control mice) when compared to control mice (145.8% ± 6.1%, n = 8). To address whether the decrease in the 10 Hz-mediated plasticity was because of a reduced eCB release, we also tested the effect of ACEA. We found that the increase in fPSP amplitude after ACEA application was strongly reduced in S.I. mice (Figure 7D; 111.5% ± 5.2%, n = 9, versus 137.8% ± 8.1%, n = 9, p = 0.017 with control mice).

Then, we directly assessed whether CB1R-sensitive inhibitory transmission was reduced by the S.I. The effect of ACEA on IPSC amplitude in control mice (Figure 7E; 76.3% ± 3.5%, n = 10) was strongly reduced in S.I. mice (91.6% ± 4.0%, n = 8, p = 0.012 compared to control). If CB1R-iLTD were induced by the social memory protocol, we predicted that CA2 PNs would be more likely to fire APs upon CA3 input stimulation. Indeed, in slices from S.I. mice, CA3 stimulation led to a large PS (Figure 7F; n = 10) in contrast to slices from control mice (n = 8, p = 0.016). These results are consistent with the premise that both the DOR- and CB1R-mediated plasticities are induced during the behavioral protocol, leading to reduced inhibitory transmission recruited by CA3 input and to enhanced AP firing.

Our results in slices suggest sequentiality between DOR and CB1R plasticities. However, it is also possible that these two plasticities are evoked simultaneously *in vivo*. To address this, we performed a single 5-min interaction with a novel mouse (5 min S.I.) and then sacrificed the test mouse within 5 min. With this protocol, a 100 Hz stimulation induced DOR plasticity (Figures 7G, 118.8% ± 4.8%, n = 17, 5 mice, p = 0.0014) that was about half the magnitude of that evoked in control mice (143.1% ± 4.4%, n = 14, 6 mice, p = 4.44 10^{-7}; p = 0.0011

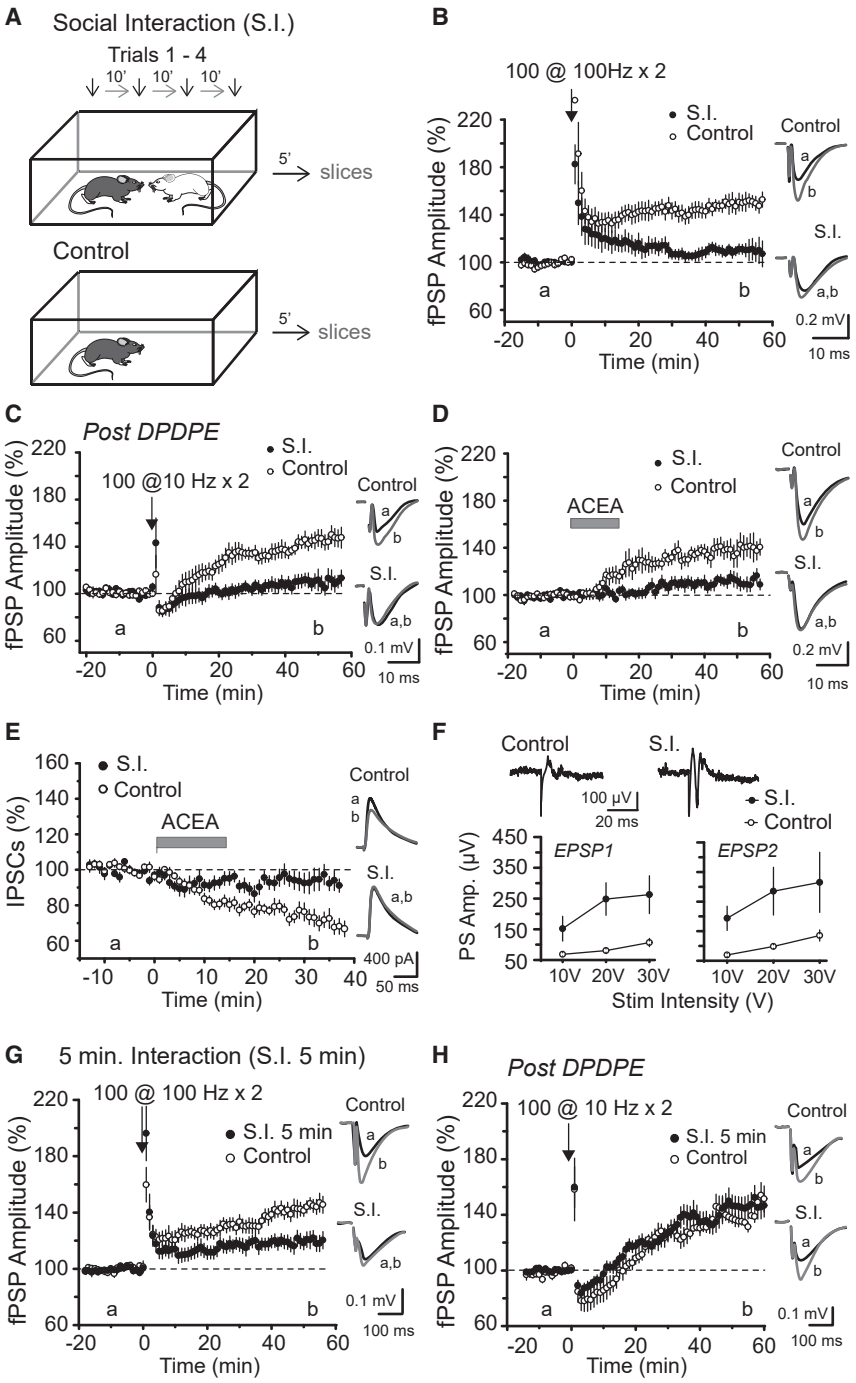

Figure 7. Social memory formation occludes CB1R-mediated plasticity

(A) Illustration of the protocol used to determine if social interaction (S.I.) occludes DOR and CB1R-mediated plasticities in area CA2.

(B) Summary graph of normalized CA3-CA2 fPSP before and after a 100 Hz stimulation (100 pulses at 10 Hz) in control mice (open circles, n = 9) and in S.I. mice (filled circles, n = 8; p = 6.66 10^{-4} comparison with control mice). Right: averaged fPSP traces corresponding to the time points before (a) and after (b) stimulation.

(C) Summary graph of normalized CA3-CA2 fPSP amplitude before and after a 10 Hz stimulation (100 pulses at 10 Hz) in control mice (open circles, n = 8) and in S.I. mice (filled circles, n = 11; p = 5.8 10^{-4} comparison with control mice). Right: averaged fPSP traces.

(D) Summary graph of normalized CA3-CA2 fPSP before and after application of the CB1R agonist ACEA in control mice (open circles, n = 9) and in S.I. mice (filled circles, n = 9; p = 0.017 comparison with control mice). Right: averaged fPSP traces.

(E) Summary graph showing that application of ACEA in presence of AMPA and NMDA receptor blockers induced a lasting decrease in the IPSC amplitude in control mice (open circles, n = 10) but not in S.I. mice (filled circles, n = 8; p = 0.012 comparison with control mice). Right: averaged IPSC traces. Cells were held at +10 mV throughout the experiment.

(F) Summary graphs of the amplitude of the population spike monitored in the somatic layer of area CA2 in response to a paired stimulation of CA3 input in control conditions (open circles, n = 8) and after S.I. (filled circles, n = 10; p = 0.016 comparison with control mice). Top: averaged traces.

(G and H) Summary graph of normalized CA3-CA2 fPSP before and after a 100 Hz stimulation (G; control n = 14, S.I. n = 17, p = 0.0011) or a 10 Hz stimulation (H; control n = 5, S.I. n = 15, p = 0.691) following a single 5-min S.I. Right: averaged fPSP traces. Error bars denote SEM.

with S.I. 5 min), indicating that DOR-iLTD was partially occluded. In contrast, when we provided a 10 Hz stimulation to induce CB1R plasticity, the increase in fPSP was identical between 5 min S.I. (Figure 7H; 146.7% ± 7.3%, n = 15) and control mice (141.4% ± 4.0%, n = 5, p = 0.691 with S.I. 5min). Altogether, these data strongly support a role for CB1R plasticity in social memory formation, and they indicate that the sequentiality of DOR and CB1R plasticity occurs *in vivo* during social memory formation.

CB1-plasticity is impaired in the 22q11.2 DS mouse model and rescued by a manipulation that rescues social memory

In the mouse model of 22q11.2 deletion syndrome (DS), social recognition memory is impaired (Piskorowski et al., 2016). This impairment likely results from the fact that CA2 PNs are more hyperpolarized in these mice, thus preventing AP firing, even following DOR-iLTD. We thus asked if CB1-plasticity is altered in these mice. In wild-type (WT) littermate controls, a 10 Hz stimulation after DPDPE incubation induced a large increase in the fPSP (Figure 8A; 165.8% ± 18.4%, n = 8, p = 0.008). In contrast, a 10 Hz stimulation induced a small increase in the fPSP amplitude in slices from 22q11.2DS mice (LgDel; Figure 8A; 114.7% ± 3.7%, n = 11; p = 0.005).

This impairment could be explained by the fact that CA2 PNs are more hyperpolarized in 22q11.2DS mice, firing fewer APs

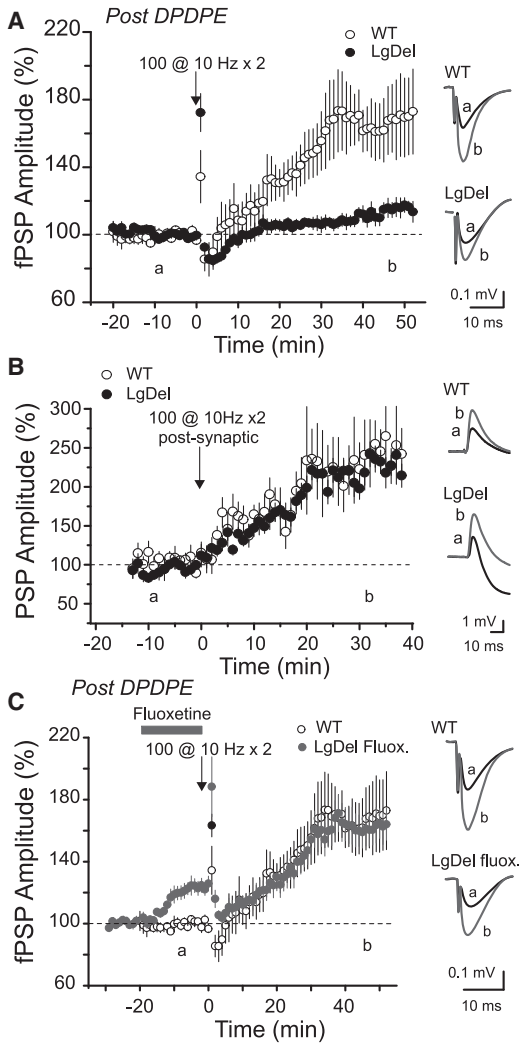

Figure 8. CB1-plasticity is impaired in the 22q11.2 DS mouse model

(A) Summary graph of normalized CA3-CA2 fPSP amplitude before and after a 10 Hz stimulation in WT (open circles, n = 8, p = 0.008) and LgDel (filled circles, n = 11, p = 0.005) mice. Right: averaged fPSP traces corresponding to the time points before (a) and after (b) stimulation.

(B) Summary graph of normalized CA3-CA2 PSP amplitude recorded in whole-cell before and after a post-synaptic 10 Hz stimulation in WT (open circles, n = 10, p = 3.56 10^{-4}) and in LgDel mice (filled circles, n = 11, p = 6.34 10^{-7}). Cells were maintained at −70 mV throughout the experiment. Right: averaged PSP traces.

(C) Summary graph of normalized CA3-CA2 fPSP amplitude before and after 10Hz stimulation. The 10 Hz stimulation provided at the end of the TREK channel blocker application (fluoxetine 100 μM) induced an increase in fPSP amplitude in LgDel mice (gray-filled circles, n = 8, p = 8.1 10^{-4}) that was similar to that observed in WT mice (open circles, n = 8, p = 4.7 10^{-4}), same experiments as panel A). Right: averaged fPSP traces. Error bars indicate the SEM in all panels. See also Figure S6.

during the induction protocol and not releasing eCBs. Alternatively, the molecular pathways underlying CB1R-mediated plasticity could be impaired. To address this point, we performed whole-cell recordings and used the 10 Hz depolarizing protocol to force AP firing in the PN. With this protocol, the disinhibitory increase in the PSP amplitude was identical between WT and LgDel mice (Figure 8B; WT: 226.1% ± 21.4%, n = 10, 10 mice, p = 3.56 10^{-4}; LgDel: 216.2% ± 10.3%, n = 11, 8 mice, p = 6.34 10^{-7}, p = 0.68 between WT and LgDel). Thus, the impairment in CB1-plasticity in LgDel mice likely results from an impairment in AP firing and not from impaired signaling downstream of CB1R activation. Therefore, CB1-plasticity could potentially be rescued in LgDel mice assuming that PNs fire enough APs during the induction protocol.

CA2 PNs are more hyperpolarized in 22q11.2DS mice because of a higher conductance through the K^+ leak channel, TREK-1 (Piskorowski et al., 2016). Reducing TREK-1 conductance in CA2 PNs can restore social memory in 22q11.2DS mice (Donegan et al., 2020). Thus, we postulated that blocking TREK-1 channels may restore CB1R plasticity. We induced DOR plasticity with DPDPE, then recorded fPSPs and applied fluoxetine to block TREK-1 channels. Fluoxetine application induced a small increase in the fPSP (Figure 8C; 122.2% ± 4.2%, n = 8, p = 8.1 10^{-4}). We then applied a 10 Hz stimulation of CA3 inputs at the end of fluoxetine application to induce CB1R plasticity. This protocol resulted in a large increase in the fPSP amplitude (Figure 8C; 161.9% ± 10.4%, n = 8, p = 4.7 10^{-4}) that was indistinguishable from that evoked in WT mice (p = 0.86). This increase was not due to a lasting effect of fluoxetine because in separate experiments a 10 min fluoxetine application only transiently increased the fPSP amplitude (Figure S6A; 116.7% ± 5.2%, n = 5, p = 0.043). Blocking TREK-1 channels likely permits plasticity induction because it allows PNs to fire APs. Indeed, while almost no PS was evoked after DOR plasticity in LgDel mice, fluoxetine application was sufficient to reveal AP firing in response to CA3 input stimulation (Figure S6B). Altogether, these data are consistent with a role of CB1R plasticity in social memory formation. Not only is CB1R plasticity altered in a mouse model with impaired social memory, it can also be rescued by a manipulation that was shown to rescue social memory, i.e., depolarization of CA2 PNs through TREK-1 blockade.

DISCUSSION

Two forms of inhibitory plasticity coexist in area CA2 of the hippocampus

Inhibitory transmission in area CA2 expresses a unique iLTD mediated by DOR activation that decreases GABA release from PV+ INs (Piskorowski and Chevaleyre, 2013a). Here we show that in addition to DOR-iLTD, another inhibitory LTD can also be induced in area CA2. This iLTD is mediated by CB1R activation, and in agreement with the described CB1R expression in the hippocampus (Katona et al., 1999), this plasticity does not involve PV+ INs, but likely CCK+ INs. The mechanism of CB1R-iLTD in CA2 differs in several important ways from that in CA1. In CA1, glutamate release from neuronal activity results in activation of mGluR-I, leading to release of the eCB 2-AG independently of intracellular [Ca^{2+}] increase in PNs (Chevaleyre and Castillo, 2003). In area CA2, however, our results indicate that mGluR-I activation does not trigger eCB release and blockade of all mGluRs does not prevent CB1R plasticity. Instead, we show that the release of eCBs requires an increase in intracellular

[Ca^{2+}] and AP firing by CA2 PNs was sufficient to evoke CB1R-iLTD. This dependence on AP firing explains why a 100 Hz stimulation protocol is ineffective in evoking CB1R-iLTD, as CA2 PNs intrinsically fire at 10–15 Hz (Robert et al., 2020) and fire only a few APs during a 100 Hz stimulation.

The peculiar mode of eCB release in area CA2 has important consequences for the expression of the plasticity. In contrast to CA1, CB1R-iLTD is not input specific, but likely only occurs on synapses targeting CA2 PNs that fire APs (Figure S7). Another peculiarity of CB1R-iLTD in area CA2 is that it was induced only after DOR-iLTD induction. This is because CA3 inputs can only evoke AP firing in CA2 PNs once the feedforward inhibition is reduced by DOR-iLTD. Recently, it was shown in area CA1 that the *in vivo* activity of PV+ and CCK+ IN ensembles is inversely coupled, and that PV+ INs inhibit CCK+ INs (Dudok et al., 2021). Our results demonstrate a consequence of this segregation of activity, as the DOR-iLTD is limited to PV+ INs and can be induced with a single exposure to a novel conspecific. This reduction in PV+ transmission then allows for CA2 PN firing and a reduction of CCK+ transmission with further exposures to the novel animal.

Role of CB1R-dependent plasticity in social memory formation

Previous studies have suggested that DOR-iLTD plays a role in social memory formation, a form of memory critically dependent on CA2 PN AP firing. However, pharmacological blockade of DORs in area CA2 only slightly reduced social memory (Leroy et al., 2017), and genetic deletion of DORs (Domínguez et al., 2019) delayed, but did not prevent, social memory formation. Our results indicate that CB1R-iLTD also plays a role in social memory formation. However, we cannot discard the possibility that CB1Rs are involved in social memory independently of the plasticity observed in CA2. We hypothesize that the DOR plasticity must occur before the CB1R plasticity *in vivo* based on our finding that a single social interaction can occlude DOR plasticity but has no effect on CB1R plasticity. Interestingly, while DOR-iLTD is observed in every recorded CA2 PN (Piskorowski and Chevaleyre, 2013a), we found that AP firing was enhanced primarily in superficial CA2 PNs. In area CA1, deep and superficial PNs differ by their intrinsic properties, their level of inhibition from PV + interneurons, and their synaptic targets (Soltesz and Losonczy, 2018). It is currently unknown what underlies the facilitated firing in superficial CA2 PNs after DOR plasticity induction. However, differences in firing or in connectivity have also been reported *in vivo* along the radial axis (Oliva et al., 2016) and the proximodistal axis (Fernandez-Lamo et al., 2019). Therefore, our results strengthen the idea that different subpopulations of CA2 PNs contribute differently to hippocampal activity and function.

Manipulation that restores social memory formation also restores CB1R plasticity in the 22q11.2 mouse model

Here we found that CB1R-iLTD could not be induced in 22q11.2DS mice with stimulation of CA3 inputs but was induced when AP firing was driven with whole-cell current injection. In 22q11.2DS mice, PNs are more hyperpolarized because of an increased conductance through TREK-1 K^+ channels (Piskorowski et al., 2016). Decreasing TREK-1 channel conductance in CA2 PNs of 22q11.2DS mice was sufficient to restore social memory (Donegan et al., 2020). TREK-1 channel blockers likely act on every PN but probably induce firing only in some of them, hence potentially altering CA2 network function. However, this action is only transient and cannot account for maintenance of coding. Our results show that by allowing CB1R plasticity to be induced, the action of the TREK channel blocker is not only amplified but also maintained over a longer period of time. Interestingly, inhibitory transmission in area CA2 is disrupted from CCK+, but not from PV+ INs, in the Neuroligin 3 knockout mouse (Modi et al., 2019), a mouse model of autism with social memory impairments, suggesting that CB1-plasticity could be altered in these mice. Altogether, these data strongly support a role for CB1R plasticity in social memory formation and highlight how potential treatments that would favor CB1R plasticity in area CA2 could be used to improve social memory impairment observed in psychiatric or neurodegenerative diseases.

STAR★METHODS

Detailed methods are provided in the online version of this paper and include the following:

- KEY RESOURCES TABLE
- RESOURCE AVAILABILITY
  - Lead contact
  - Materials availability
  - Data and code availability
- EXPERIMENTAL MODEL AND SUBJECT DETAILS
- METHOD DETAILS
  - Slice preparation
  - Electrophysiological recordings and analysis
  - Electrophysiology following social memory protocol
  - Mice were sacrificed 5 min after the social interaction
  - Immunohistology and analysis
  - Intra-CA2 cannulas implantation and injection procedure
  - Behavioral experiments
  - Histological control of intra-CA2 injections
- QUANTIFICATION AND STATISTICAL ANALYSIS

SUPPLEMENTAL INFORMATION

Supplemental information can be found online at https://doi.org/10.1016/j.neuron.2022.06.013.

ACKNOWLEDGMENTS

This work was supported by Agence National de la Recherche (ANR-18-CE16-0006 and ANR-18-CE37-0020), Fondation pour la Recherche Médicale (Equipe FRM EQU202003010457). Confocal imaging was carried out at NeuroImag imaging core facility at IPNP. We acknowledge the Mouse Behavioral Core (MBC-CBI-ANEXPLO, Toulouse, France) for its expertise and assistance in setting up behavioral apparatus and procedures. The cacng5-cre mouse line and the DREADD AAV vectors were a kind gift from the McHugh lab at RIKEN. The LgDel mouse line was kindly provided by Francesco Papaleo's lab at the Fondazione Istituto di Tecnologia.

AUTHOR CONTRIBUTIONS

Conceptualization, M.L., V.C., R.A.P., and L.V.; Investigation, M.L., G.B., S.L., M.M., A.S., J.D., R.A.P., and V.C.; Formal analysis, M.L., V.C., and L.V.; Writing, M.L., V.C., R.A.P., and L.V.

DECLARATION OF INTERESTS

The authors declare no competing interests.

Received: September 21, 2021
Revised: April 22, 2022
Accepted: June 10, 2022
Published: July 19, 2022

REFERENCES

Benes, F.M., Kwok, E.W., Vincent, S.L., and Todtenkopf, M.S. (1998). A reduction of nonpyramidal cells in sector CA2 of schizophrenics and manic depressives. Biol Psychiatry *44*, 88–97. https://doi.org/10.1016/s0006-3223(98)00138-3.

Boehringer, R., Polygalov, D., Huang, A.J.Y., Middleton, S.J., Robert, V., Wintzer, M.E., Piskorowski, R.A., Chevaleyre, V., and McHugh, T.J. (2017). Chronic Loss of CA2 transmission leads to hippocampal Hyperexcitability. Neuron *94*, 642–655.e9. e9. https://doi.org/10.1016/j.neuron.2017.04.014.

Chevaleyre, V., and Castillo, P.E. (2003). Heterosynaptic LTD of hippocampal GABAergic synapses. Neuron *38*, 461–472. https://doi.org/10.1016/s0896-6273(03)00235-6.

Chevaleyre, V., and Siegelbaum, S.A. (2010). Strong CA2 pyramidal neuron synapses define a powerful disynaptic cortico-hippocampal loop. Neuron *66*, 560–572. https://doi.org/10.1016/j.neuron.2010.04.013.

Chevaleyre, V., Takahashi, K.A., and Castillo, P.E. (2006). Endocannabinoid-mediated synaptic plasticity in the CNS. Annu. Rev. Neurosci. *29*, 37–76. https://doi.org/10.1146/annurev.neuro.29.051605.112834.

Chiang, M.-C., Huang, A.J.Y., Wintzer, M.E., Ohshima, T., and McHugh, T.J. (2018). A role for CA3 in social recognition memory. Behav. Brain Res. *354*, 22–30. https://doi.org/10.1016/j.bbr.2018.01.019.

Domínguez, S., Rey, C.C., Therreau, L., Fanton, A., Massotte, D., Verret, L., Piskorowski, R.A., and Chevaleyre, V. (2019). Maturation of PNN and ErbB4 signaling in area CA2 during adolescence underlies the emergence of PV interneuron plasticity and social memory. Cell Rep. *29*, 1099–1112.e4. e4. https://doi.org/10.1016/j.celrep.2019.09.044.

Donegan, M.L., Stefanini, F., Meira, T., Gordon, J.A., Fusi, S., and Siegelbaum, S.A. (2020). Coding of social novelty in the hippocampal CA2 region and its disruption and rescue in a 22q11.2 microdeletion mouse model. Nat. Neurosci. *23*, 1365–1375. https://doi.org/10.1038/s41593-020-00720-5.

Dudok, B., Klein, P.M., Hwaun, E., Lee, B.R., Yao, Z., Fong, O., Bowler, J.C., Terada, S., Sparks, F.T., Szabo, G.G., et al. (2021). Alternating sources of perisomatic inhibition during behavior. Neuron *109*, 997–1012.e9. e9. https://doi.org/10.1016/j.neuron.2021.01.003.

Fernandez-Lamo, I., Gomez-Dominguez, D., Sanchez-Aguilera, A., Oliva, A., Morales, A.V., Valero, M., Cid, E., Berényi, A., and Menendez de la Prida, L. (2019). Proximodistal Organization of the CA2 hippocampal area. Cell Rep. *26*, 1734–1746.e6. e6. https://doi.org/10.1016/j.celrep.2019.01.060.

Hefft, S., and Jonas, P. (2005). Asynchronous GABA release generates long-lasting inhibition at a hippocampal interneuron-principal neuron synapse. Nat. Neurosci. *8*, 1319–1328. https://doi.org/10.1038/nn1542.

Hitti, F.L., and Siegelbaum, S.A. (2014). The hippocampal CA2 region is essential for social memory. Nature *508*, 88–92. https://doi.org/10.1038/nature13028.

Karayiorgou, M., Simon, T.J., and Gogos, J.A. (2010). 22q11.2 microdeletions: linking DNA structural variation to brain dysfunction and schizophrenia. Nat. Rev. Neurosci. *11*, 402–416. https://doi.org/10.1038/nrn2841.

Katona, I., Sperlágh, B., Sik, A., Käfalvi, A., Vizi, E.S., Mackie, K., and Freund, T.F. (1999). Presynaptically located CB1 cannabinoid receptors regulate GABA release from axon terminals of specific hippocampal interneurons. J. Neurosci. *19*, 4544–4558. https://doi.org/10.1523/jneurosci.19-11-04544.1999.

Knable, M.B., Barci, B.M., Webster, M.J., Meador-Woodruff, J., and Torrey, E.F.; Stanley Neuropathology Consortium (2004). Molecular abnormalities of the hippocampus in severe psychiatric illness: postmortem findings from the Stanley Neuropathology Consortium. Mol. Psychiatry *9*, 609–620. 544. https://doi.org/10.1038/sj.mp.4001471.

Kogan, J.H., Franklandand, P.W., and Silva, A.J. (2000). Long-term memory underlying hippocampus-dependent social recognition in mice. Hippocampus *10*, 47–56. https://doi.org/10.1002/(sici)1098-1063(2000)10:1<47::aid-hipo5>3.0.co;2-6.

Leroy, F., Brann, D.H., Meira, T., and Siegelbaum, S.A. (2017). Input-timing-dependent plasticity in the hippocampal CA2 region and its potential role in social memory. Neuron *95*, 1089–1102.e5. e5. https://doi.org/10.1016/j.neuron.2017.07.036.

Mehta, M.R. (2015). From synaptic plasticity to spatial maps and sequence learning. Hippocampus *25*, 756–762. https://doi.org/10.1002/hipo.22472.

Meira, T., Leroy, F., Buss, E.W., Oliva, A., Park, J., and Siegelbaum, S.A. (2018). A hippocampal circuit linking dorsal CA2 to ventral CA1 critical for social memory dynamics. Nat. Commun. *9*, 4163. https://doi.org/10.1038/s41467-018-06501-w.

Modi, B., Pimpinella, D., Pazienti, A., Zacchi, P., Cherubini, E., and Griguoli, M. (2019). Possible Implication of the CA2 hippocampal circuit in social cognition deficits observed in the Neuroligin 3 knock-out mouse, a non-Syndromic animal model of autism. Front Psychiatry *10*, 513. https://doi.org/10.3389/fpsyt.2019.00513.

Moy, S.S., Nadler, J.J., Dold, G., Trang, D., Simmons, N., Perez, A., Young, N.B., Barbaro, R.P., Piven, J., Magnuson, T.R., and Crawley, J.N. (2004). Automated apparatus for quantitation of social approach behaviors in mice. Gene Brain Behav. *3*, 303–314. https://doi.org/10.1111/j.1601-183x.2004.00071.x.

Nasrallah, K., Piskorowski, R.A., and Chevaleyre, V. (2015). Inhibitory plasticity permits the Recruitment of CA2 pyramidal neurons by CA3. eNeuro *2*. ENEURO.0049–15.2015. https://doi.org/10.1523/ENEURO.0049-15.2015.

Nasrallah, K., Therreau, L., Robert, V., Huang, A.J.Y., McHugh, T.J., Piskorowski, R.A., and Chevaleyre, V. (2019). Routing hippocampal information flow through parvalbumin interneuron plasticity in area CA2. Cell Rep. *27*, 86–98.e3. https://doi.org/10.1016/j.celrep.2019.03.014.

Oliva, A., Fernández-Ruiz, A., Buzsáki, G., and Berényi, A. (2016). Role of hippocampal CA2 region in triggering Sharp-Wave Ripples. Neuron *91*, 1342–1355. https://doi.org/10.1016/j.neuron.2016.08.008.

Piskorowski, R.A., and Chevaleyre, V. (2013a). Delta-opioid receptors mediate unique plasticity onto parvalbumin-expressing interneurons in area CA2 of the Hippocampus. J. Neurosci. *33*, 14567–14578. https://doi.org/10.1523/JNEUROSCI.0649-13.2013.

Piskorowski, R.A., and Chevaleyre, V. (2013b). Delta-opioid receptors mediate unique plasticity onto parvalbumin-expressing interneurons in area CA2 of the Hippocampus. J. Neurosci. *33*, 14567–14578. https://doi.org/10.1523/JNEUROSCI.0649-13.2013.

Piskorowski, R.A., Nasrallah, K., Diamantopoulou, A., Mukai, J., Hassan, S.I., Siegelbaum, S.A., Gogos, J.A., and Chevaleyre, V. (2016). Age-dependent specific changes in area CA2 of the Hippocampus and social memory deficit in a mouse model of the 22q11.2 deletion syndrome. Neuron *89*, 163–176. https://doi.org/10.1016/j.neuron.2015.11.036.

Robert, V., Therreau, L., Davatolhagh, M.F., Bernardo-Garcia, F.J., Clements, K.N., Chevaleyre, V., and Piskorowski, R.A. (2020). The mechanisms shaping CA2 pyramidal neuron action potential bursting induced by muscarinic acetylcholine receptor activation. J. Gen. Physiol. *152*. https://doi.org/10.1085/jgp.201912462.

Smith, A.S., Avram, S.K.W., Cymerblit-Sabba, A., Song, J., and Young, W.S. (2016). Targeted activation of the hippocampal CA2 area strongly enhances social memory, pp. 1–8. https://doi.org/10.1038/mp.2015.189.

Soltesz, I., and Losonczy, A. (2018). CA1 pyramidal cell diversity enabling parallel information processing in the hippocampus. Nat. Neurosci. *21*, 484–493. https://doi.org/10.1038/s41593-018-0118-0.

Stevenson, E.L., and Caldwell, H.K. (2014). Lesions to the CA2 region of the hippocampus impair social memory in mice. Eur. J. Neurosci. *40*, 3294–3301. https://doi.org/10.1111/ejn.12689.

Zhao, M., Choi, Y.-S., Obrietan, K., and Dudek, S.M. (2007). Synaptic plasticity (and the lack thereof) in hippocampal CA2 neurons. J. Neurosci. *27*, 12025–12032. https://doi.org/10.1523/JNEUROSCI.4094-07.2007.

Merscher, S., Funke, B., Epstein, J.A., Heyer. J., Puech, A., Lu, M.M., Xavier, R.J., Demay, M.B., Russell, R.G., Factor, S., et al., 2001. TBX1 is responsible for cardiovascular defects in velo-cardio-facial/DiGeorge syndrome. Cell. 104(4):619-29. doi: 10.1016/s0092-8674(01)00247-1. PMID: 11239417.

STAR★METHODS

KEY RESOURCES TABLE

REAGENT or RESOURCE	SOURCE	IDENTIFIER
Chemicals, peptides, and recombinant proteins		
CGP 55845 Hydrobromide	Hello Bio	HB0960-50mg Batch: E0704-8-1
SR 95531 Hydrobromide	Tocris	Cat#1262-50mg Batch:11A/170178
D-AP5	Hello Bio	HB0225-100mg batch:E0714-4-2
DPDPE	Tocris	J66293- 5mg CAS: 88373-73-3 Lot: Q21G072
NBQX	Hello Bio	HB0443-50mg Batch:E1040-2-1
Naltrindol	Tocris	Cat#0740-10mg Batch:14A/190520
ACEA	Tocris	Cat#1319-25mg Batch:14A/232359
AM251	Hello Bio	HB2776-10mg Batch: E0637-4-6
(S)-3,5-DHPG	Hello Bio	HB0045-10mg Batch: E0791-10-3
THL	Hello Bio	HB4009-250mg batch:E1351-1-1
BAPTA	Sigma Aldrich	A4926-250mg CAS#85233-19-8 Lot: SLBW9824
Fluoxetine	Hello Bio	HB1600-50mg Batch: E0142-1-1
CPPG	Tocris	Cat#0972-10mg Batch: 12A/130814
(S)-MCPG	Tocris	Cat#0337-10mg Batch: 16*A/86419
Clozapine N-oxide (CNO)	Hello Bio	HB6149-10mg Batch: E0945-1-1
ω-Conotoxin GVIA	Hello Bio	HB1218-500μg Batch: E1660-1-1
Biocytin	Hello Bio	HB5035-50mg Batch: E1477-1-1
Far-Red Nissl	Life Technologies	Cat#N21483
Streptavidin-conjugated Alexa 594	Life Technologies	Cat#S1125
Streptavidin-conjugated Alexa 647	Life Technologies	Cat#S21374
Bacterial and virus strain		
AAV.hSyn.DIO.hM4D.Gi.mCherry	McHugh Lab	N/A
Antibodies		
Alexa Fluor™ 594 Cadaverine	ThermoFischer	A30678 - Lot: 2431320
Rabbit α-PCP4	Sigma Aldrich	HPA005792 - RRID: AB_1855086 - Lot: B97113
Alexa 555 Goat α-Rabbit	Life Technologies	A21428 - RRID: AB_2535849 - Lot: 1858260
Rat α-mCherry	Life Technologies	M11217 - RRID: AB_2536611 - Lot: QE214609
Alexa 555 Goat α-Rat	Life Technologies	A21434 - RRID: AB_2535855 - Lot: 1670155
Experimental models: Organisms/strains		
Mouse: Swiss	Janvier Labs	N/A
Mouse: C57BL/6J	Janvier Labs	N/A
Mouse model: LgDel	Merscher et al., 2001	N/A
Mouse: Swiss/J-Cacng5-Cre	McHugh Lab Boehringer et al., 2017	N/A
Mouse: B6:129P2-Pvalbtm1(cre)ArbrlJ (Pvalb-cre)	The Jackson Laboratory	Cat#017320

(*Continued on next page*)

Continued

REAGENT or RESOURCE	SOURCE	IDENTIFIER
Software and algorithms		
Axograph X software for data acquisition	Axograph	https://axograph.com
pClamp10- data acquisition	Molecular devices	https://www.moleculardevices.com
OriginPro- data analysis	Origin Lab	https://www.originlab.com
ImageJ-data analysis	ImageJ	https://imagej.net/Welcome

RESOURCE AVAILABILITY

Lead contact

Further information and requests for resources and reagents should be directed to and will be fulfilled by the lead contact, Vivien Chevaleyre (vivien.chevaleyre@parisdescartes.fr).

Materials availability

This study did not generate unique reagents.

Data and code availability

This study did not generate datasets and code.

EXPERIMENTAL MODEL AND SUBJECT DETAILS

Animals were raised in conditions that are in accordance with the Federation of European Laboratory Animal Science Associations standards. All breeding was done in an environment that was specific and opportunistic pathogen free.

All electrophysiology experiments were performed on Swiss WT or LgDel male mice (5–10 week old). C57B6J male mice (6–7 month old, Charles River, France) were used for behavioral experiments.

Mice were housed in groups of five since weaning at P21 in standard breeding cages with food and water *ad libitum* and were placed at a constant temperature (23 ± 1 °C) under diurnal conditions (light-dark: 8:00AM–8:00PM). Mice were tested during the first half of the light period. Mice were not involved in previous procedures.

All the experiments were performed in strict accordance with the recommendations of the local ethic committee and the French Ministry for Research (#2019041014597476, # 02,118.02, 2017, #2016040417305913)

METHOD DETAILS

Slice preparation

400 μm thick transverse hippocampal slices were prepared from Swiss or LgDel male mice. Animals were euthanized in accordance with institutional regulations under anesthesia with isofluorane. Mice were transcardially perfused with ice-cold solution containing (in mM): 10 NaCl, 110 sucrose, 2.5 KCl, 25 glucose, 30 NaHCO3, 20 HEPES, 1.25 NaH2PO4, 2 thiourea, 5 Na ascorbate, 3 Na pyruvate, 0.5 CaCl2 and 10 MgCl2. Hippocampi were removed and placed upright into an agar mold and cut with a vibratome (Leica VT1200S, Germany). The slices were then transferred to 30°C artificial cerebral spinal fluid (ACSF), (in mM): 125 NaCl, 2.5 KCl, 10 glucose, 26 NaHCO3, 1.25 NaH2PO4, 2 Na Pyruvate, 2 CaCl2 and 1 MgCl2 for 30 min and kept at room temperature for at least 1.5 h before recording. For experiments that required DOR-induction, slices were further incubated in a separate chamber with the DOR agonist DPDPE (0.5μM) in ACSF. All experiments were performed at 33°C.

Electrophysiological recordings and analysis

Field recordings of fPSPs were performed in current-clamp mode with a recording patch pipette (3–5 MΩ) containing 1 M of NaCl and positioned in the middle of *stratum radiatum* of CA2. Whole-cell recordings were obtained from CA2 PNs in current-clamp mode with appropriate DC current injection to maintain the cells at −70mV. Recording pipettes (3–5 MΩ) contained (in mM): 135 KMethylSulfate, 5 KCl, 0.1 EGTA-Na, 10 HEPES, 2 NaCl, 5 ATP, 0.4 GTP, 10 phosphocreatine; pH 7.2; 280–290 mOsm.

Inhibitory currents were recorded in voltage clamp mode with a patch pipette (3–5 MΩ) containing CesiumMethylSulfate in place of KMethylSulfate. For some experiments (Figure 4D), 20 mM K^+ was substituted for 20 mM BAPTA in the internal solution used for current clamp recordings.

Membrane potentials were not corrected for the liquid junction potential. Series resistance (between 12 and 18 MΩ) was monitored throughout each experiment and cells with more than 15% change were excluded from analysis.

Before beginning whole cell experiments, we identified the CA2 PNs by somatic location and size. Furthermore, the cell type was confirmed by several electrophysiological properties as previously described (Chevaleyre and Siegelbaum, 2010). Cells were also filled with biocytin and post hoc labeling of filled cells and imaging was performed to confirm CA2 recording when necessary.

Cell attached recordings were performed with ACFS in the pipette or with internal solution containing Alexa 594 conjugated cadaverine when cells were labeled at the end of the recording. AP probability was calculated by dividing the number of evoked APs by the number of CA3 input stimulation provided every 20 s (usually 10 stimulations for each intensity).

Synaptic currents or potentials were evoked by mono-polar stimulation with a broken patch pipette filled with ACSF and positioned in the middle of CA1 SR. The amplitudes of the IPSCs or EPSPs were normalized to the baseline amplitude. An HFS (100 pulses at 100Hz repeated twice, 20 s apart) or 10Hz stimulation (100 pulses at 10Hz repeated twice, 20s apart) were applied following stable baseline. The magnitude of plasticity was estimated by comparing averaged responses at 30–40 min after the induction protocol (for whole cell experiments) or 50–60 min after induction protocol (for field recording experiments) with baseline-averaged responses from 0 to 10 min before the induction protocol. We used pClamp10 and Axograph X software for data acquisition and Origin Pro for data analysis. Statistical comparisons were performed using Student's *t* test, ANOVA, Wilcoxon, Mann-Witney or Kruskal-Wallis where appropriate. All drugs were bath-applied following dilution into the external solution from concentrated stock solutions. Results are reported as mean ± SEM

Electrophysiology following social memory protocol

All mice were housed two to five in each cage and given *ad libitum* access to food and water. They were kept on a 12 h (6:00–18:00) light–dark cycle with the room temperature regulated between 21°C and 23°C. Behavioral tests were performed during the light cycle in a testing room adjunct to the mouse housing room, which minimizes any transportation stress. Immediately prior to the experimental sessions, 6 to 8 week-old mice were transferred to the testing room and placed into individual cages, identical to the ones used for housing, where they were allowed to habituate to the new environment for 10 min for 3 days. Male juvenile mice (Swiss, 4–5 weeks old) were also placed in the testing room in their home cages and allowed to habituate for a similar amount of time. Testing began when a novel juvenile mouse was introduced to a cage with one of the adult experimental mice. Activity was monitored for 10 min (trial 1 to 4, 5 min intertrial interval). The control mice were also placed in the testing room in the empty experimental cages for a similar amount of time.

Mice were sacrificed 5 min after the social interaction

Stereotaxic injection

The adeno-associated virus, AAV.DJ/8.hSyn.DIO.hM4D.GI .mCherry was used at 3 × 108 vg. 500 nL of virus was injected bilaterally into the hippocampus of 4-6 week-old cacng5-cre or Pvalb-cre mice at 100 nL/min and the injection cannula was removed 5 min after infusion was complete. Injections were centered on: AP: −1.5 mm; ML: +/−1.8 mm; at a depth of 1.5 mm from the brain surface. The resulting infected area spanned at least 2 mm along the longitudinal axis of the hippocampus.

Immunohistology and analysis

Recorded cells were filled with biocytin and post-hoc labeling of filled cells with streptavidin-conjugated Alexa 488 was performed along with immunohistology to confirm cell identity. Gi-DREADD-mcherry was labeled with rat α-dsRed (Life Technologies) diluted 1:2000 and Cy3-goat α-rat. PCP4 was labeled with rabbit α-PCP4 (Sigma) and Alexa 555-conjugated anti rabbit (Life Technologies). For cell-attached recordings Alexa 594-conjugated cadaverine (Life technologies) was included in the pipette and filled the cells after recording.

In order to assess if CA2 pyramidal cells were deep or superficial, all neuronal soma were stained with a far-red conjugated nissl (Neurotrace, Life Technologies). Slices were mounted with Pro-Long Diamond (Thermofisher) and z series confocal images were collected with a Zeiss 710 LSM microscope. Image analysis was performed with ImageJ and cellular morphologies were reconstructed from confocal images with Neurolucida 360 (MicroBrightField).

Intra-CA2 cannulas implantation and injection procedure

One week prior the behavioral testing, 6–7 months old C57B6J male mice (n = 28; Charles River, France) were anesthetized with isoflurane (1%–4%) and placed in a stereotaxic instrument (Kopf, CA). All animals were then implanted bilaterally with 7 mm stainless-steel guide cannulas (gauge: 24; diameter: 0.56 mm) positioned 1 mm above the injection site in the area CA2 at the following coordinates: AP −1.98 mm; L ±2.3 mm; and DV −2 mm relative to bregma. The guide cannulas were then anchored to the skull using dental cement. Stainless-steel wire inlet cannulas (7 mm) were placed inside to prevent occlusion. The bilateral infusions were performed with stainless-steel injector needles (length: 8 mm; gauge: 31; diameter: 0.28 mm) inserted inside the guide cannulas and fitted so that they protruded 1 mm below, into the area CA2. The injectors were connected via a polyethylene catheter (Tygon) to 1 μL Hamilton microsyringes fitted to a micropump (Harvard apparatus). For injection into dorsal CA1, the guide cannulas were placed at the following coordinate: AP −1.75 mm; L ±1.4 mm; DV −1.65 mm relative to bregma.

AM251 (3μg/0.25μL) or its vehicle (10% Cremophor-EL; 10% DMSO; 80% NaCl 0.9%) solutions were bilaterally injected into the area CA2 of the hippocampus at a volume of 0.25 μL/side and a flow rate of 0.1 μL/min. Mice were gently maintained by hand on a foam board to allow the experimenter to control the volume and prevent injector needle to move out of the cannula throughout the

injection. Before behavioral testing, the injector needle was left in the guide cannula for one additional minute to allow fluid diffusion.

Behavioral experiments

All the experiments were performed in strict accordance with the recommendations of the European Union (86/609/EEC) and the French National Committee (87/848). The seven-trial social memory test is based on a modified version from Kogan et al. (2000). Briefly, on test day 1, immediately after injection of AM251 or its vehicle, each mouse was first placed in a large chamber (25 × 35 cm) for 10 min habituation with an empty cylindrical small cage placed in the center (8 cm diameter). Then a stimulus mouse (Mouse A), from same age and sex, but never encountered before, was introduced in the small cage for four successive trials of 5 min (ITI 10 min). On the fifth trial, a novel stimulus mouse was introduced (Mouse B). On test day 2, the same stimulus mouse as day 1 (Mouse A) was presented again for two other 5 min trials following the exact same procedure as day 1 (10 min of habituation; 10 min ITI), but with no intracerebral injections.

Two weeks prior to the seven-trial social memory test, a subset of animals (n = 15) was used to assess the effect of intra-CA2 injection of AM251 or its vehicle on sociability. Briefly, immediately after injection, the mice were placed for 10 min of habituation in an empty three-chamber setup (Moy et al., 2004). To assess sociability, mice were then placed in the presence of a littermate (familiar) mouse confined in a cylindrical cage with bars (8cm diameter) on one side, and an identical cylindrical cage on the opposite side of the three-chamber apparatus. The location of the familiar mouse was counterbalanced between experimental groups. After a 2 weeks wash-out period, mice which received AM251 or its vehicle during the sociability test received the same treatment during the seven-trial social memory test.

For all the behavioral experiments, the direct interactions were scored online by the experimenter. All apparatus and testing chambers were cleaned with 70% ethanol between animals.

Histological control of intra-CA2 injections

Mice were deeply anesthetized with dolethal solution (ip) before being transcardially perfused with saline solution for 30–45 s. The brains were removed, post-fixed in 4% paraformaldehyde and phosphate buffer 0.1M for 48 h at 4 °C before being transferred into a 30% sucrose and 0.1% sodium azide solution. 40-μm-thick-coronal sections were cut with a sliding microtome (Leica SM2010R) equipped with a freezing-stage (Physitemp BFS-3MP). Sections were placed on a gelatinated slide and counter-stained with cresyl violet.

QUANTIFICATION AND STATISTICAL ANALYSIS

We used Origin Pro for data analysis. We used a Shapiro-Wilk test to determine whether the data followed a normal distribution. We used Student's t tests and ANOVA when the data followed a normal distribution. When the distribution was not normal, we used non-parametric test (Wilcoxon, Man-Whitney and Kruskal-Wallis tests). Statistical significance was set to $p < 0.05$ (*** indicates $p < 0.001$, ** indicates $p < 0.01$, and * indicates $p < 0.05$). All values are reported as the mean ± SEM.